

Optical, structural, and photocatalytic properties of Cd-doped ZnO powders prepared via sol–gel method

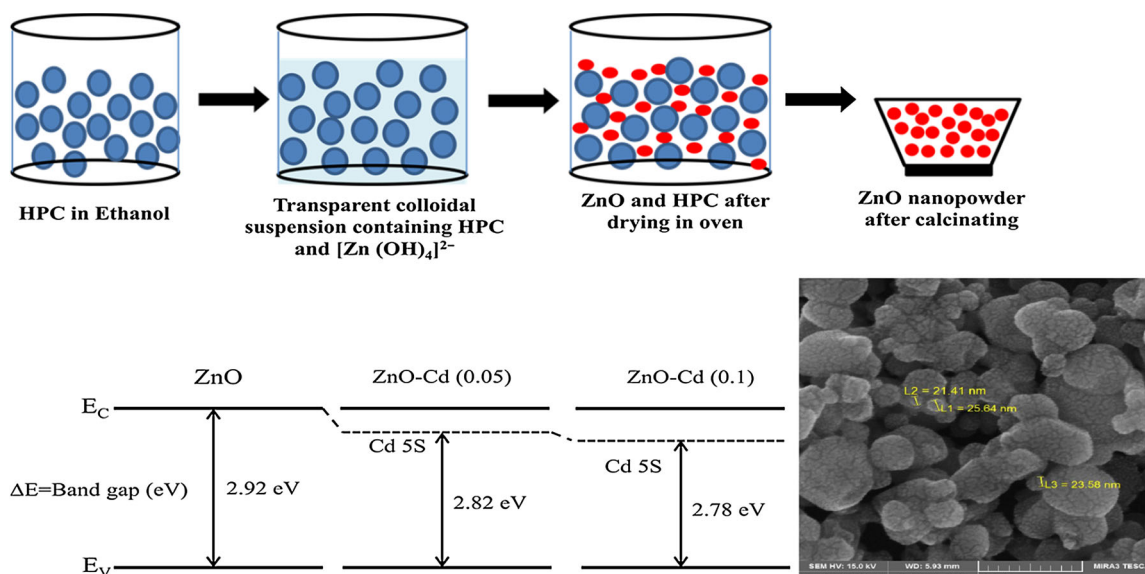
Bahar Khodadadi¹ · Maryam Bordbar¹ · Ali Yeganeh-Faal²

Received: 15 June 2015 / Accepted: 21 September 2015 / Published online: 7 October 2015
© Springer Science+Business Media New York 2015

Abstract In the present study, undoped ZnO and Cd–ZnO nanostructures with different weight ratios of cadmium were synthesized by the sol–gel method. Structural and optical properties were investigated by Fourier transform spectroscopy, UV–Vis spectroscopy, scanning electron microscopy, energy-dispersive analytical X-ray, X-ray diffraction, and photoluminescence spectroscopy methods. Moreover, the direct band gap is calculated by

Tauc's approach. Furthermore, photocatalytic activity of all samples has been investigated under UV irradiation in an aqueous medium. Compared with pure ZnO, the band gap of the Cd–ZnO decreases and depends on the content of dopants. In addition, photocatalytic activity improves in the presence of a small amount (5 wt%) of cadmium dopant.

Graphical Abstract



✉ Bahar Khodadadi
Bkhodadadi98@yahoo.com; Khodadadi@qom.ac.ir

¹ Department of Chemistry, Faculty of Science, University of Qom, Qom, Iran

² Department of Chemistry, Faculty of Science, Payam Noor University, Qom, Iran

Keywords ZnO–Cd nanopowder · Band gap · Photocatalytic activity · Sol–gel method

1 Introduction

Zinc oxide (ZnO) is an n-type semiconductor with a wide direct band gap of 3.37 eV and a high excitation binding energy of approximately 60 meV [1–4]. Due to its unique properties, ZnO can be used for many applications in pigments, gas sensors, optical devices, solar cells, and photocatalysis [5, 6]. Beside the simplicity and low-cost aspects in the proposed preparation strategy, ZnO is an important material for applications in both fundamental and applied research [7]. However, the band gap energies are large (about 3.2 eV), which means ZnO can only be excited for photocatalytic uses under UV light which forms only 4 % of the solar spectra, greatly impeded the photocatalytic efficiency of these photocatalysts in the direct use of solar light. Thus, two major challenges in using these photocatalysts are broadening of the light response region and improvement in their stability [8, 9].

Therefore, doping transitional metal ions offers promising opportunities in order to shift the optical absorption of ZnO into the visible region and prevent charges from the recombination on the photocatalyst surfaces [10, 11].

Considering its proportional abundance and low cost, cadmium is a good candidate as a dopant. By doping Cd on ZnO, its absorption edge could be red-shifted. In fact, Cd incorporation can affect not only the band gap, but also the n-type carrier concentration. This is reasonable because Cd^{2+} has an ionic radius of (0.78 Å) close to that of Zn^{2+} (0.60 Å) and the stable wurtzite phase of ZnO is conserved on doping with Cd [12–14].

Several methods have been employed for the synthesis of ZnO. Among the various chemical techniques, sol–gel process is a promising method for the preparation of nanomaterials, because of the notable advantages of high purity, good homogeneity, low-temperature synthetic conditions, low equipment cost, and easily controlled reaction parameters [15, 16].

Although several experimental studies have been reported on synthesis via sol–gel method and properties of ZnO–Cd nanofilms, there are few reports on the properties of ZnO–Cd nanopowder [17–20]. The main reason is that sol–gel method is mostly used for the preparation of nanofilms. In this work, in order to investigate the influence of Cd-doping level on the optical, structural, morphological, and photocatalytic properties of ZnO nanopowder, ZnO and Cd-doped ZnO nanopowders (with different weight ratios) were synthesized via the sol–gel method. Moreover, hydroxylpropyl cellulose (HPC) is used as organic polymer for preventing agglomeration of nanopowders and modifying photocatalytic activity. The absorption spectra of the samples were measured, and the

variations in the optical band gap were analyzed. Morphology and sample structures were investigated by IR spectra, scanning electron microscopy (SEM), and X-ray diffraction (XRD) methods.

2 Experimental

2.1 Materials and equipments

Zinc acetate ($\text{Zn}(\text{CH}_3\text{COO})_2$), diethanolamine (DEA), hydroxylpropyl cellulose (HPC), absolute ethanol, double-distilled water, ethanol, cadmium nitrate tetrahydrate ($\text{Cd}(\text{NO}_3)_2 \cdot 4\text{H}_2\text{O}$), and acetone (for drying) were obtained from Merck Chemical Company.

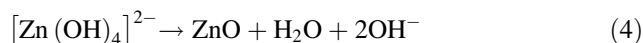
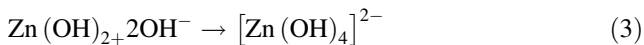
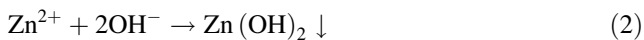
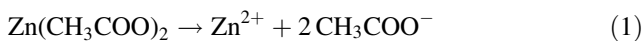
The ZnO sample structures were characterized by X-ray diffraction pattern recorded on a Philips model X'Pert Pro diffractometer employing Cu K α radiation ($\lambda = 1.5418 \text{ \AA}$), while the morphologies of the synthesized samples were investigated by field emission scanning electron microscopy (FESEM; TESCAN-MIRA3) equipped with an Oxford INCA energy-dispersive X-ray detector. UV–Vis absorption spectra were recorded by using a Shimadzu UV-2500 spectrophotometer in the wavelength range of 200–700 nm. Fourier transform infrared (FTIR) spectra were obtained using the FTIR (Jasco, 4200) with the KBR method.

2.2 Sample preparation

In a typical synthesis, undoped ZnO and Cd–ZnO samples were synthesized by the following procedure:

First, 0.2 g HPC was dissolved in 30 mL absolute ethanol and stirred for 10 min using a homogenizer. 0.02 mol $\text{Zn}(\text{CH}_3\text{COO})_2$ was then added to the solution, and stirring was continued for 15 min at 60 °C (solution I). Next, $\text{Cd}(\text{NO}_3)_2 \cdot 4\text{H}_2\text{O}$ was dissolved in 5 mL absolute ethanol (with weight ratio of dopant/Zn = 0.00, 0.05, and 0.10), followed by the addition of 0.2 mL double-distilled water and 0.8 mL diethanolamine (DEA) to solution and stirring for 5 min (solution II). Finally, solution II was added dropwise into solution I and the resulting solution was vigorously stirred for 30 min at 60 °C. The obtained transparent colloidal suspension was aged 72 h to allow a gel to form. The sample was dried in an oven at 50 °C and ultimately calcinated at 500 °C for 4 h.

On the basis of these results, the growth of ZnO could be proposed based on the chemical reactions involved and crystal growth habits of ZnO. The reaction process can be expressed as follows:



The reaction (2) could be easily observed when adding DEA to the Zn^{2+} solution. As more of the DEA solution was added, the $\text{Zn}(\text{OH})_2$ precipitate dissolved to yield a homogenous solution containing $[\text{Zn}(\text{OH})_4]^{2-}$ ions. Upon increasing the time further, ZnO nuclei formed from the dehydration of $[\text{Zn}(\text{OH})_4]^{2-}$ ions and followed by crystal growth [21]. Moreover, in order to illuminate the effect of the HPC as organic polymer on synthesis, steps are summarized in Fig. 1.

3 Results and discussion

3.1 Sample characterization

Fourier transform infrared (FTIR) spectroscopy was carried out for the characterization of functional groups at room temperature in the range of 400–4000 cm^{-1} , and the results are shown in Fig. 2. The broad absorption band at $\sim 3435 \text{ cm}^{-1}$ is related to the O–H stretching vibrations of water present in ZnO. Another small absorption peak at $\sim 1635 \text{ cm}^{-1}$ can be associated with the bending vibrations of H_2O molecules. Thus, there are some hydroxyl groups on the surface of ZnO. In addition, the strong absorption band between 400 and 600 cm^{-1} corresponds to the stretching and vibrational modes of metal–oxygen (M–O). Very small peaks originated at 891 cm^{-1} may be due to the nitrate (NO_3^-) groups [22].

Moreover, the stretching mode of ZnO nanostructure appears at 546 cm^{-1} . The broad peak observed in the 460–560 cm^{-1} range is the combination of Zn–O vibrations [23]. The vibration mode at 475 cm^{-1} has changed

slightly in doped samples. It seems that the change is related to interaction between ZnO and metal ions, which have formed new bonds [24].

Based on FTIR spectra, no obvious changes are observed in the spectra of undoped and doped samples (with weight ratio of Cd/Zn = 0.05 or 0.10).

The X-ray diffraction patterns of samples are shown in Fig. 3. The diffraction patterns of ZnO sample well match with JCPDS card of ZnO (No. 01-080-0074). The XRD pattern of samples can be indexed to those of hexagonal wurtzite structure [5, 25].

Comparing the spectrum of pure ZnO with those of samples doped with 5 and 10 wt% Cd indicates that the

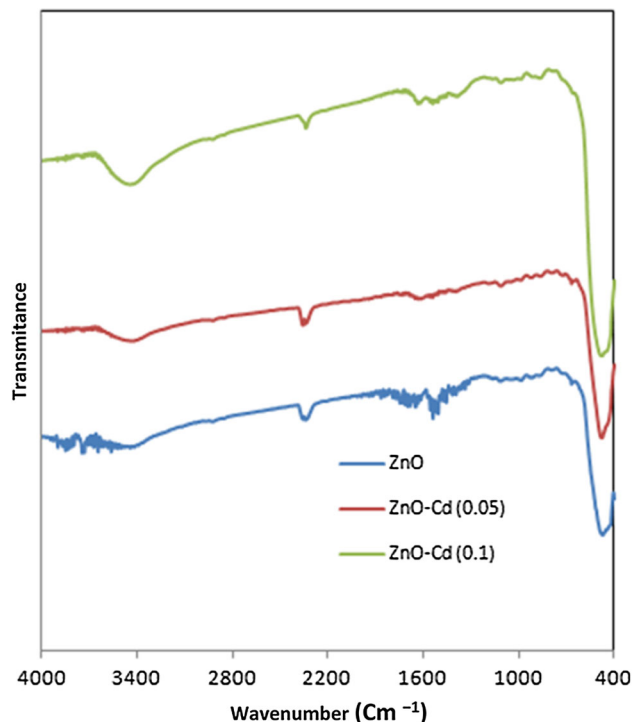


Fig. 2 FTIR spectra of undoped and Cd–ZnO samples

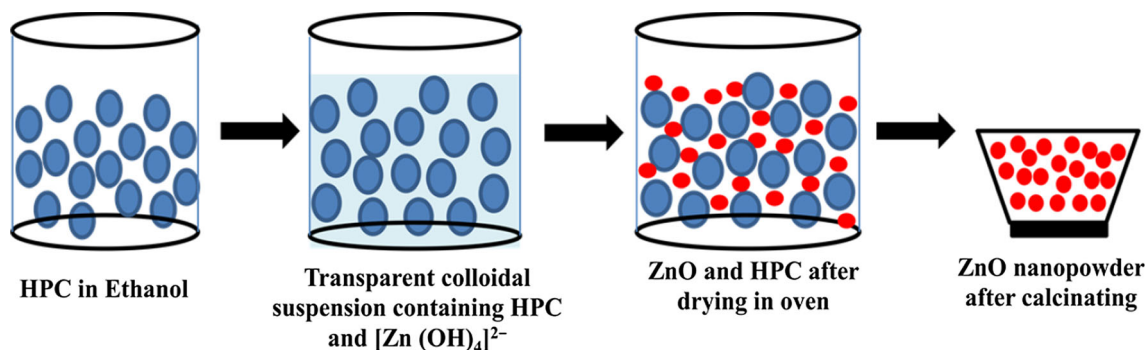


Fig. 1 Diagrammatic synthesis of ZnO nanopowder in the presence of HPC via sol-gel method

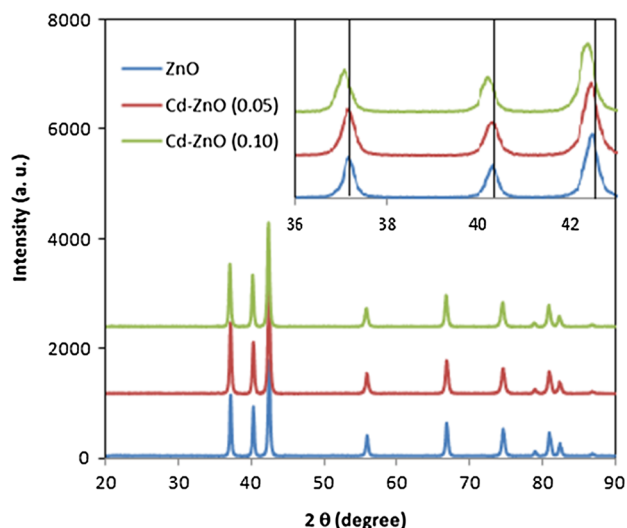


Fig. 3 XRD spectrum and peak position shifting of undoped and Cd-ZnO samples

samples are single phase with a hexagonal wurtzite without a formation of impurities like CdO. The diffraction peaks of Cd-ZnO samples are shifted to lower angles with the increasing Cd concentration. The shift of peaks to lower values is reasonable because the ionic radius of Cd^{2+} (0.78 Å) is larger than that of Zn^{2+} (0.60 Å) at tetrahedral site. This shift also indicates the expansion of lattice by forming Cd-ZnO solid solutions [26].

Table 1 Peak position, band gap, and lattice constants of samples

Samples	EDAX analysis (Cd %)	$a_{(100)}$	$c_{(002)}$	Wavelength (nm)	Band gap (eV)
ZnO	0.0	3.2517	5.2033	369	2.92
Cd-ZnO (0.05)	4.3	3.2468	5.2061	378	2.82
Cd-ZnO (0.10)	9.1	3.2527	5.2139	380	2.78

The lattice parameters of ZnO and Cd-ZnO with different concentrations were calculated from the XRD using the following equation [16].

$$\frac{1}{d^2} = \frac{4}{3} \left(\frac{h^2 + kh + k^2}{a^2} \right) + \frac{l^2}{c^2}$$

Table 1 shows the calculated lattice parameters of the samples. Lattice parameters of Cd-ZnO are slightly more than those of ZnO, confirming that the Cd ions have been doped into the ZnO crystal lattice without changing the wurtzite structure. On the other hand, zinc and cadmium have ionic radii of 0.78 and 0.60 Å, respectively. Hence, if Cd replaces Zn in the ZnO crystal lattice, an increase in lattice parameters is expected. As shown in Table 1, the c-axis lattice parameter increases from 5.2033 to 5.2061 and 5.2139 Å, respectively, as the dopant level increases from 0 to 10 wt%, indicative of Cd atoms replacing zinc atoms in the ZnO lattice [27, 28].

In order to determine the morphologies of ZnO, SEM analysis has also been carried out. All samples are of similar size and morphology [10]. Figure 4a illustrates a typical FESEM image of the ZnO-Cd (0.05) sample. Further evidence of the formation of Cd-ZnO came from the energy-dispersive analytical X-ray (EDAX) analysis (Fig. 4b). Based on these results, the samples are composed of Zn, Cd, and O, also based on EDAX analysis results, the concentration of Cd has been estimated, and result is shown in Table 1.

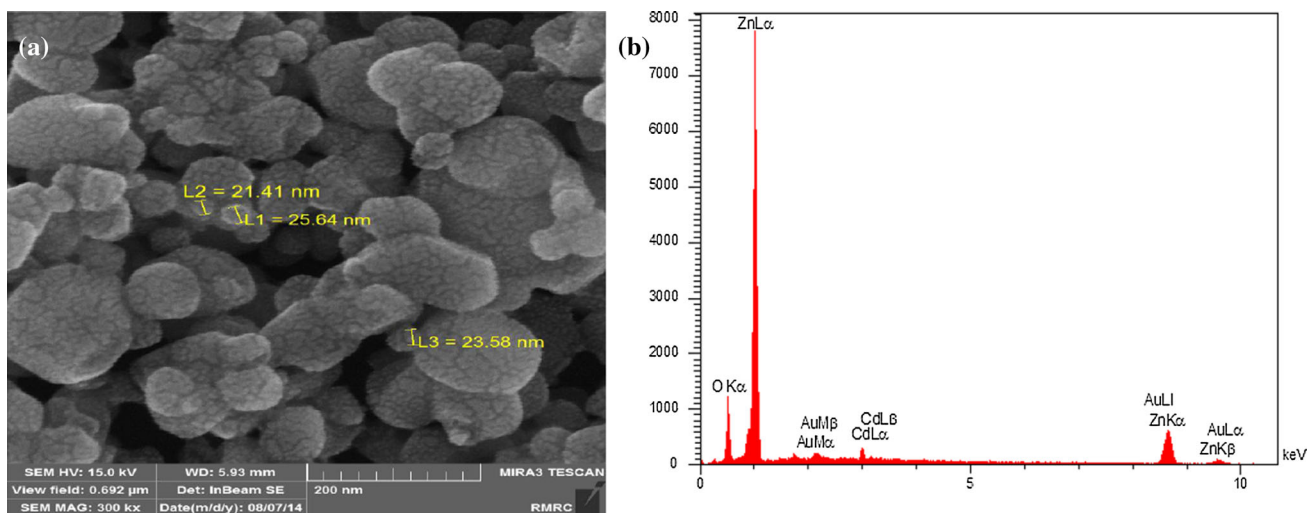


Fig. 4 a FESEM image and b EDAX analysis of ZnO-Cd (0.05) sample

3.2 Optical properties of samples

UV–Vis absorption spectroscopy was performed to investigate the optical properties of synthesized samples. In order to record absorption UV–Vis spectra, a very small amount of samples were dispersed in absolute ethanol by means of sonication bath (33 kHz, 350 W) at room temperature. Figure 5a shows the UV–Vis absorption spectra of undoped and Cd²⁺-doped ZnO with different dopant concentrations. It can be clearly seen that the different synthesized ZnO nanostructures exhibit a single and well-defined absorption band at 369 nm, which is the characteristic band for the wurtzite hexagonal structure of ZnO. Moreover, the maximum of the absorbance band shifts slightly toward higher wave lengths due to cadmium doping and increase in dopant content. The wavelengths of maximum absorbance for each nanostructure sample are listed in Table 1.

The absorption coefficients of samples were investigated by Tauc’s approach, and the optical band gap of the undoped and Cd²⁺-doped ZnO rods with various Cd²⁺ contents was calculated using the following equation:

$$(\alpha h\nu)^2 = C(h\nu - E_g)$$

where α is the absorption coefficient, C is a constant, $h\nu$ is the photon energy, and E_g is the band gap. Figure 5b shows the Tauc plots of samples. Extrapolation of the linear region of Tauc’s plot gives a band gap [29].

The band gap of the doped samples (Table 1) is smaller than that of undoped ZnO and decreases with increasing concentration of cadmium. The band gaps were calculated to be 2.92, 2.85, and 2.78 eV corresponding to the different Cd/Zn values of 5 and 10 wt%.

There are two primary causes that may contribute to variations in band gap energies. It is reasonable to expect the slight band gap (E_g) to decrease with increase in concentrations of Cd possibly due to doping-induced band edge bending [30–32]. Moreover, these results indicate that the band gap reduction of ZnO–Cd samples is due to the formation of Cd 5 s state below the CB edge [26]. Energy diagram of samples is shown in Fig. 5c.

Figure 6 shows the room temperature photoluminescence spectroscopy (PL) spectra of the samples. According to PL spectra, mainly two photoluminescence peaks could

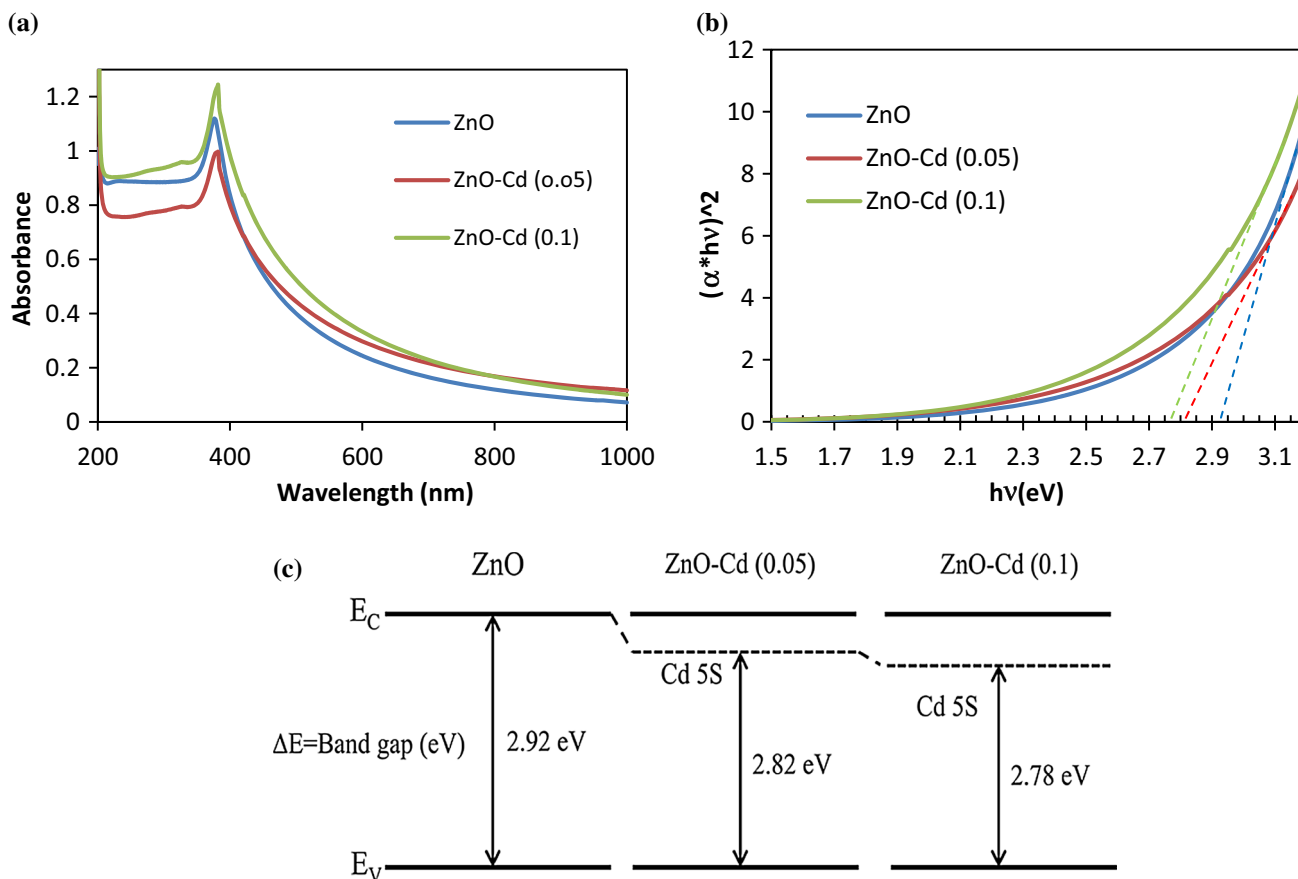


Fig. 5 a UV–Vis absorption spectrum, b the Tauc plots, and c energy diagram of samples

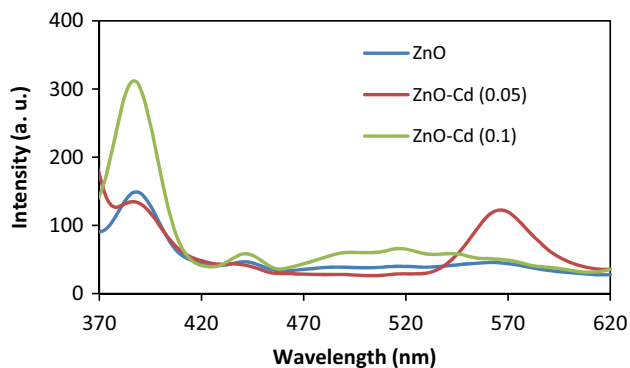


Fig. 6 Photoluminescence spectra of undoped and Cd–ZnO samples

be observed: a 380-nm ultraviolet peak attributed to the near-band edge emission (NBE), which comes from the collision of the free excited electrons and holes, and one quite weak visible emission band at around 520–570 nm, known as the deep-level emission (DLE) mediated by oxygen vacancies and other defects. As shown in Fig. 6, all samples have two peaks at about 380 and 570 nm [33–35].

Since PL emission is the result of the recombination of excited electrons and holes, the lower PL intensity of the prepared ZnO indicates a lower recombination rate of excited electrons and holes [36]. After doping 5 wt% of Cd into the ZnO, the near-band edge emission (NBE) peak intensity decreases, whereas the deep-level emission (DLE) peak intensity increases. The relative photoluminescence intensity of the NBE to blue emission or deep-level emission (DLE) (INBE/IDLE) reduces from 3.1 to 1.1 on doping ZnO with Cd at 5 wt%. This may be due to inhibition of recombination of the photogenerated electron–hole pairs on doping ZnO with Cd [37].

However, on further increasing the Cd content (10 wt%), the near-band edge emission (NBE) peak intensity and (INBE/IDLE) increase (6.3) in comparison with ZnO–Cd (5 wt%) probably due to more recombination rate, which is in good agreement with the calculated band gap. Additionally, peak centering at about 445 nm just for ZnO–Cd (0.1) sample was caused by the transition between the vacancies of oxygen and interstitial oxygen. Also, the broad peak centering about 515 nm originated from the ionized oxygen vacancies in the valance, and weak peak centering at about 547 nm was also observed, which corresponded to the transition of oxygen vacancies [38].

3.3 Photocatalytic activity

Photocatalytic activities of the samples were measured by the degradation of MO as a model reaction and the effects of various Cd-doping concentrations from 0 to 10 wt% on the photocatalytic activity were investigated. The results are shown in Fig. 7 [39, 40].

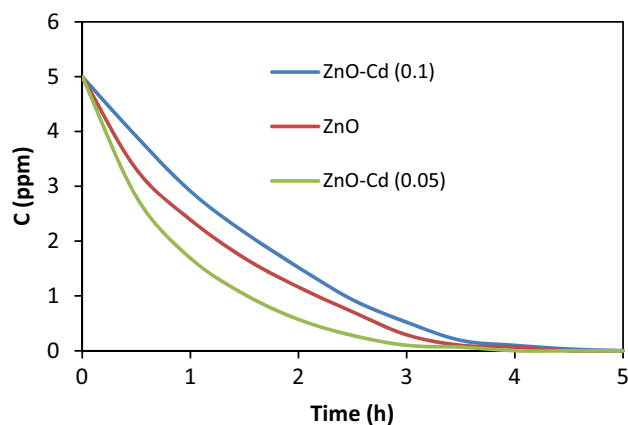


Fig. 7 Photodegradation of methyl orange (MO) using the samples

Methyl orange (MO) degradation was evaluated as follows: 5 mg of the samples was dispersed in 1000 mL solution. Before the illumination, the suspensions were magnetically stirred in the dark for 1 h to ensure the establishment of absorption equilibrium of methyl orange on the sample surfaces. After that, suspension was irradiated under a 50-W low-pressure Hg lamp. UV–Vis absorption spectra were recorded at different times to calculate MO concentration.

It can be observed that when a 5 wt% of Cd is doped into the ZnO, the photocatalytic activity increases in comparison with the undoped ZnO, but further increases in the dopant concentration result in a decrease in photocatalytic activity [40].

It is well known that modifying the band of the semiconductor and hindering the recombination of photogenerated electrons and holes and increased surface active sites are important factors contributing to the enhancement of the photocatalytic activity. Moreover, the lattice defects such as oxygen vacancy could serve as favorable trap sites of the electrons or holes to reduce their recombination and consequently increase the photocatalytic activities [41, 42].

ZnO–Cd (5 wt%) nanostructure exhibited more effective electron–hole separation under UV light irradiation. Hence, the surface redox process by photogenerated electrons and holes occurs more easily and the photocatalytic activity of ZnO has significantly improved correspondingly [39].

Since the incorporation of Cd ions into ZnO photocatalyst decreases the reduction potential of electrons or causes lattice distortion of ZnO, the photocatalytic activity has to be reduced by further addition of cadmium [43].

It should be also noted that for ZnO–Cd photocatalysts of high Cd contents, the excessive Cd particles may occupy the active surface sites of photocatalysts and obstruct the incident light to a certain extent, causing the inferior efficiencies of these photocatalysts (ZnO–Cd 10 wt%).

4 Conclusions

Zinc oxide nanopowder doped with cadmium was synthesized by a sol–gel method and used as a catalyst in the process of photodegradation of methyl orange as a dye model. According to the results, the red shift in band edge absorption peak in UV–Vis absorbance spectrum with increasing metal content observed verifies the doping of metal in ZnO nanostructure. Moreover, the band gap of samples was analyzed by Tauc’s approach and calculations confirmed that application of cadmium ion as a dopant and dopant concentration is very effective on band gap of ZnO. Based on the experimental results obtained in this study, the existence of a small amount of cadmium in ZnO structure enhances the photodegradation efficiency, but further increases in the dopant concentration result in a decrease in photocatalytic activity.

Acknowledgments We gratefully acknowledge the University of Qom and the Payam Noor University for the support of this work.

References

- Bao J, Zimmler MA, Capasso F (2006) *Nano Lett* 6:1719–1722
- Bai XD, Gao PX, Wang ZL, Wang EG (2003) *App Phys Lett* 82:4806–4808
- Lin HF, Liao SC, Hung SW (2005) *J Photoch Photobiol A* 174:82–87
- Amornpitoksuk P, Suwanboon S, Sangkanu S, Sukhoom A, Muensit N (2012) *Baltrusaitis. J Powder Technol* 219:158–164
- Zhou X, Li Y, Peng T, Xie W, Zhao X (2009) *Mater Lett* 63:1747–1749
- Suwanboon S, Amornpitoksuk P, Sukolrat A, Muensit N (2013) *Ceram Int* 39:2811–2819
- Yousef A, Nasser A, Barakat M, Amna T, Afeesh R (2012) *J Lumin* 132:1668–1677
- Liua C, Liua Z, Li Y, Liua Z, Wang Y, Lei E, Ya J, Gargiulo N, Caputo D (2012) *Mater Sci Eng, B* 177:570–574
- Liu G, Li G, Qiu X, Li L (2009) *J Alloy Compd* 481:492–497
- Xu C, Cao L, Su G, Liu W, Qu X, Yu Y (2010) *J Alloy Compd* 497:373–376
- Talebian N, Nilforoushan MR, Malek N (2013) *Thin Solid Films* 527:50–58
- Tang X, Lu H, Zhang Q, Zhao J, Lin Y (2011) *Solid State Sci* 13:384–387
- Mahmoud WE, Al-Ghamdi AA, El-Tantawy F, Al-Heniti S (2009) *J Alloys Compd* 485:59–63
- Karunakaran C, Vijayabalan A, Manikandan G (2012) *Superlattic Microst* 51:443–453
- Tian J, Wang J, Dai J, Wang X, Yin Y (2009) *Surf Coat Tech* 204:723–730
- Zhong J, Zhang Li J, Yang He X, Zeng J, Lu Y, Hu W, Lin K (2012) *Curr Appl Phys* 12:998–1001
- Yakuphanoglu F, Ilcan S, Caglar M, Caglar Y (2010) *Superlattice Microst* 47:732–743
- Thomas D, Abraham J, Vattappalam SC, Augustine S, Thomas D (2014) *Indo Am J Pharm Res* 4:1612–1616
- Dong ZY, Li YF, Yao B, Ding ZH, Yang G, Deng R, Fang X, Wei ZP, Liu L (2014) *J Phys D: App Phys* 47:1–6
- Duan L, Zhao X, Wang Y, Shen H, Geng W, Zhang F (2015) *J Alloy Compd* 645:529–534
- Sin JC, Lam SM, Lee KT, Mohamed AR (2013) *Ceram Int* 39:5833–5843
- Ni YH, Wei XW, Hong JM, Ye Y (2005) *Mater Sci Eng, B* 121:42–47
- Lin J, Lin J, Zhu YF (2007) *Inorg Chem* 46:8372–8378
- Ghosh CK, Malkhandi S, Mitra MK, Chattopadhyay KK (2008) *J Phys D: App Phys Lett* 41:245113
- Saravanan R, Karthikeyan S, Gupta VK, Sekaran G, Narayanan V, Stephen A (2013) *Mat Sci Eng C* 33:91–98
- Anandan S, Ohashi N, Miyauchi M (2010) *Appl Catal B-Environ* 100:502–509
- Liu XC, Shi EW, Chen ZZ, Zhang HW, Xiao B, Song LX (2006) *Appl Phys Lett* 88:252501–252503
- Hea R, Hockingb RK, Tsuzukia T (2012) *Mater Chem Phys* 132:1035–1040
- Fu H, Pan C, Yao W, Zhu Y (2005) *J Phys Chem B* 109:22432–22439
- Al-Hajry A, Umar A, Hahn YB, Kim DH (2009) *Superlattice Microst* 45:529–534
- Wu C, Huang Q (2010) *J Lumin* 130:2136–2141
- Fu M, Li Y, Wua S, Lu P, Liu J, Dong F (2011) *Appl Surf Sci* 258:1587–1591
- Li Q, Kang Z, Mao B, Wang E, Wang C, Tian C, Li S (2008) *Mater Lett* 62:2531–2534
- Long T, Takabatake K, Yin S, Sato T (2009) *J Cryst Growth* 311:576–579
- Majeed J, Jayakumar OD, Mandal BP, Salunke HG, Naik R, Tyagi AK (2014) *J Alloy Compd* 597:95–100
- Sun JH, Dong SY, Feng, Yin XJ, Zhao XC (2011) *J Mol Catal A: Chem* 335:145–150
- Karunakaran C, Gomathisankar P, Manikandan G (2010) *Mater Chem Phys* 123:585–594
- Jia T, Wang W, Long F, Fu Z, Wang H, Zhang Q (2009) *J Alloy Compd* 484:410–415
- Wang L, Hu Q, Li Z, Guo J, Li Y (2012) *Mater Lett* 79:277–280
- Ba-Abbad MM, Kadhum AAH, Mohamad AB, Takriff MS, Sopian K (2013) *Chemosphere* 91:1604–1611
- Wen M, Cheng M, Zhou S, Wu Q, Wang N, Zhou L (2012) *J Phys Chem C* 116:11702–11708
- Yamamoto S, Watarai H (2008) *J Phys Chem C* 112:12417–12424
- Whang TJ, Hsieh MT, Chen HH (2012) *Appl Surf Sci* 258:2796–2801